THE JOURNAL OF PHYSICAL CHEMISTRY A

pubs.acs.org/JPCA Article

Observation of π-Backbonding in a Boronyl-Coordinated Transition Metal Complex $TaBO^-$

Published as part of The Journal of Physical Chemistry virtual special issue "Cheuk-Yiu Ng Festschrift".

Joseph Czekner and Lai-Sheng Wang*

Cite This: *J. Phys. Chem. A* 2020, 124, 10001−10007 Read Online

ABSTRACT: The boronyl anion (BO^-) is isoelectronic to CO and CN^-, but its metal complexes are rare. Here we report the observation of a boronyl complex with an early transition metal ($TaBO^-$) produced by a laser vaporization supersonic cluster source. Its electronic structure and chemical bonding are investigated by photoelectron imaging and theoretical calculations. Vibrationally resolved photoelectron spectra of $TaBO^-$ are obtained for several low-lying electronic states of neutral TaBO and the electron affinity of TaBO is measured to be 1.729(2) eV. Theoretical calculations show that the ground states of $TaBO^-$ ($^4\Delta$) and TaBO ($^5\Delta$) are both linear with high spin multiplicities. Natural atomic orbital analyses reveal that π-backbonding is present in both $TaBO^-$ and TaBO. This study presents the first observation of π-backbonding to a boronyl ligand and suggests that early transition metals may be good candidates to form boronyl complexes.

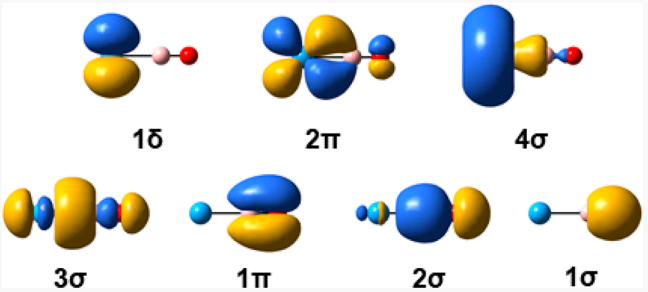

1. INTRODUCTION

The boronyl anion (BO^-) is isoelectronic to CN^- and CO.[1] While CN^- and CO are important inorganic ligands, the chemistry of boronyl and BO^- is much less known. In addition to its strong polarity and high chemical reactivity, BO^- is not a good π acceptor compared to the well-known CN^- and CO ligands,[1] because its π^* lowest unoccupied molecular orbital (LUMO) is much higher in energy. Thus, even though it is a strong σ donor, boronyl metal complexes have lower thermodynamic stability relative to those of the well-known CN^- and CO ligands. Boronyl as a ligand is much more stable in the gas phase than in solution and has been observed in a number of gaseous molecules and clusters. The H_3C-BO molecule was first characterized experimentally in the gas phase by photoelectron spectroscopy (PES).[2] Since then, many compounds with BO units have been studied experimentally and theoretically, as reviewed briefly in a recent account.[3]

The BO units were first observed as distinct structural features in small boron-rich oxide clusters.[4−7] The high stability of the BO unit was also found in larger boron-rich oxide clusters, where BO units were observed to be bonded to the periphery of planar boron cluster cores[8−12] or form bridged bonds analogous to boranes.[13] However, much less is known about metal complexes with BO ligands. The $Au_n(BO)^-$ (n = 1−3) clusters were produced and investigated by PES and theoretical calculations[14] and they represented the first gaseous metal-BO complexes to be characterized. The Au−B bonding was found to be similar to the H−B bonding, and the $AuBO^-$ cluster was shown to have a covalent Au−B bond with no π-backbonding. A subsequent theoretical study on $Au(BO)_2^-$ shows that it is isoelectronic to the well-known $Au(CN)_2^-$ anion.[15] More recently, two main group metal boronyl complexes, $BiBO^-$ and BiB_2O^-, have been observed and investigated.[16,17] A lanthanide diboronyl complex, $Ce(BO)_2^-$, has also been reported.[18] Very recently, several transition metal boronyl complexes have been reported.[19,20] In RhB_2O^-,[19] the boronyl ligand is found to be coordinated to Rh, which forms a terminal quadruple bond with B. However, in ReB_2O^- the boronyl unit is found to be bonded to the second B atom,[20] which forms a terminal triple bond with Re, similar to that in BiB_2O^-.[17] The chemical reactivities of the BO radical with organic molecules have also been investigated in crossed molecular beam experiments under single collision conditions.[21−23] The first boronyl metal complex to be synthesized in the bulk involved a BO ligand coordinated to a Pt atom, which was also protected by other bulky ligands.[24] This

Received: October 9, 2020
Revised: November 9, 2020
Published: November 19, 2020

https://dx.doi.org/10.1021/acs.jpca.0c09196
J. Phys. Chem. A 2020, 124, 10001−10007

landmark work has stimulated significant further interests in boronyl chemistry.[25−38]

In the current study, we report the observation of a gaseous transition metal boronyl species, $TaBO^-$, which is characterized by photoelectron imaging (PEI) and theoretical calculations. The electron affinity (EA) of TaBO is measured to be 1.729 eV. The bending and Ta−B stretching frequencies of the linear TaBO in its $^5\Delta_0$ ground state are measured to be 250 and 320 cm^{-1}, respectively. The frequency of the Ta−B stretching mode in the $^3\Delta_1$ excited state of TaBO is also measured (310 cm^{-1}). Theoretical calculations show π-backbonding is present from Ta to BO despite the high energy of the π^* orbital, indicating that tantalum and other early transition metals may be well suited for the syntheses of boronyl complexes.

2. EXPERIMENTAL METHODS

The experiments were performed with a high-resolution PEI apparatus, which has been described previously.[39] Anions were generated by laser vaporization of a mixed target made of Ta, isotopically enriched ^{11}B, and Ag. Clusters formed in the source were cooled through supersonic expansion with a He carrier gas seeded with 10% Ar. Anions in the cluster beam were analyzed by time-of-flight mass spectrometry. We found that residual oxygen on the surface of the target was sufficient to produce the $TaBO^-$ anion, which was selected and allowed to enter the imaging lens for photodetachment. Two laser systems were used for the PEI experiment in the current study: a Nd:YAG laser at 532.0 nm and an OPO system tuned to 647.67 nm. Photoelectrons were focused onto a microchannel plate coupled to a phosphorus screen and charged-coupled device (CCD) camera. The repeller voltages used on the imaging lens for the 532.0 and 647.67 nm experiments were −800 and −300 V, respectively. Each spectrum required approximately one million laser shots to achieve a satisfactory signal-to-noise ratio due to the relatively weak mass intensity. The spectra were calibrated using Au^- at several photon energies. The photoelectron images were processed using the Maximum Entropy Velocity Legendre Reconstruction (MEVELER) program.[40]

3. THEORETICAL METHODS

Calculations were performed using the Gaussian 09 program suite[41] to assist spectral interpretation. Previous studies showed that the ordering of the electronic states for TaCO, which is isoelectronic to $TaBO^-$ and $TaCN^-$, depends on the methods and basis sets used.[42−45] Therefore, we have done calculations using multiple levels of DFT (B3LYP,[46,47] PBE1PBE,[48−50] PW91PW91,[51] and BP86[52,53]) using the 6-31++g(d,p)[54,55] and aug-cc-pVTZ[56] basis sets for boron and oxygen and LANL2DZ[57,58] and Stuttgart[59] basis sets including effective core potentials and full relativistic effects for Ta. We included two additional f-type polarization functions and one g-type polarization function for the Stuttgart basis set as recommended by Martin and Sundermann,[60] which previously produced good results for boron-doped tantalum clusters.[61−63] We also performed CCSD(T)[64−66] single-point calculations using the optimized structures from the optimized PW91PW91 and BP86 geometries with the same basis sets. ADEs were determined by taking the difference of the zero-point corrected energies of the optimized neutral and anion states for the DFT results. No zero-point corrections were applied to the CCSD(T) calculations because only single-point calculations were done. The zero-point corrections were similar for the neutral and anion structures, so they should not have a large effect on the CCSD(T) calculations.

4. EXPERIMENTAL RESULTS

The reconstructed images and spectra of $TaBO^-$ at 647.67 and 532.0 nm are displayed in Figure 1. The spectrum in Figure 1a shows three strong peaks (X, A, and B), each followed by a short vibrational progression. Peaks X, A, and B represent the 0−0 transitions of three spin−orbit states derived from the $^5\Delta$ ground state of TaBO (*vide infra*) and their electron binding energies are given in Table 1. The vibrational features from peaks A and B have clearly defined doublet splitting, while those for peak X are not well resolved. Three more transitions (C−E) are observed in the 532.0 nm spectrum (Figure 1b), where short vibrational progressions are also assigned for D and E. Two weak features, X′ and A′, are observed in both spectra below 1.71 eV due to vibrational hot bands. A full summary of the peak positions and assignments is given in Figure S1 and Table S1 of the Supporting Information.

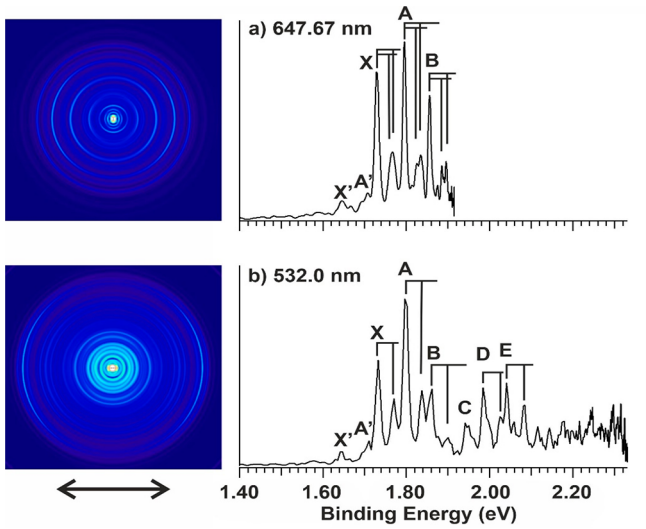

Figure 1. Photoelectron spectra of $TaBO^-$ at (a) 647.67 nm (1.9143 eV) and (b) 532.0 nm (2.331 eV). Vertical lines show the assigned vibrational progressions.

5. THEORETICAL RESULTS

The possible geometries for the triatomic system include the linear or bent TaBO, TaOB, and BTaO structures and their anions, which were all calculated with different spin multiplicities. The boronyl-related structures, $TaBO^-$ and $TaOB^-$, and a bent isomer were found to be stable minima, but we could not locate a minimum for the Ta-insertion species BTaO. The linear $TaBO^-$ with a quartet spin state ($^4\Delta$) was found to be the lowest in energy from all of the methods used, although certain levels of theory showed a sextet state ($^6\Sigma^+$) could be competitive. The $TaOB^-$ and bent structures were found to be much higher in energy (>20 kcal/mol) and were excluded from consideration. Single-point CCSD(T) calculations indicated that the $^4\Delta$ state of $TaBO^-$ is more stable than the $^6\Sigma^+$ state by 14.9 kcal/mol (Table 2). The relative energies for the different electronic states of $TaBO^-$ and TaBO

https://dx.doi.org/10.1021/acs.jpca.0c09196
J. Phys. Chem. A 2020, 124, 10001−10007

Table 1. Summary of Experimental Results and Calculated ADEs[a]

peak	transition	BE (eV)	ADE (eV)[b]	ΔE (cm^{-1})	frequencies (cm^{-1}) ν_2	ν_3	β[c]
X′	$^5\Delta_0 \leftarrow {}^4\Delta_{3/2}$	1.646(4)	–	−670(30)	–	–	–
A′	$^5\Delta_1 \leftarrow {}^4\Delta_{3/2}$	1.707(3)	–	−180(20)	–	–	–
X	$^5\Delta_0 \leftarrow {}^4\Delta_{1/2}$	1.729(2)	1.65[1.64]	0	250(30)	320(40)	1.4[0.7]
A	$^5\Delta_1 \leftarrow {}^4\Delta_{1/2}$	1.795(2)	–	530(20)	240(20)	320(30)	1.3[0.9]
B	$^5\Delta_2 \leftarrow {}^4\Delta_{1/2}$	1.856(2)	–	1020(20)	240(20)	320(20)	0.8[0.5]
C	$^3\Sigma^+ \leftarrow {}^4\Delta_{1/2}$	1.947(4)	2.26[1.86]	1760(30)	–	–	0.5
D	$^3\Delta_0 \leftarrow {}^4\Delta_{1/2}$	1.987(3)	2.62[2.28]	2080(20)	–	310(30)	0.6
E	$^3\Delta_1 \leftarrow {}^4\Delta_{1/2}$	2.041(3)	–	2520(20)	–	330(20)	0.5

[a]Peak labels correspond to Figure 1, ΔE is the energy relative to peak X, and β is the anisotropy parameter. Numbers in parentheses represent the experimental uncertainty. [b]These values are calculated using BP86 with the Stuttgart basis set for Ta and aug-cc-pVTZ basis set for B and O. The values in the brackets are calculated using CCSD(T) with the same basis sets using the optimized geometries from the BP86 calculations. See Table S4 for all calculated ADEs. [c]The values in the brackets are the anisotropy parameters from the spectrum in Figure 1a; all others are from Figure 1b.

Table 2. Calculated Molecular Properties for Low-Lying Electronic States of $TaBO^-$ and TaBO[a]

molecule	state	R(Ta−B/C) (Å)	R(B−O/C−N) (Å)	$\langle S^2\rangle$	ΔE[b] (kcal/mol)	calculated freq (cm^{-1}) (ν_1, ν_2, ν_3)
$TaBO^-$	$^2\Pi$	2.212	1.250	0.946[c]	11.1 (11.5)	1667, 267, 336
	$^4\Delta$	2.223	1.248	3.750	0.0 (0.0)	1683, 266, 329
	$^6\Sigma^+$	2.244	1.249	8.750	4.2 (14.9)	1674, 264, 325
TaBO	$^3\Sigma^+$	2.167	1.232	2.000	14.0 (5.0)	1774, 254, 360
	$^3\Delta$	2.196	1.232	2.011	22.3 (14.8)	1770, 257, 350
	$^5\Delta$	2.110	1.232	6.000	0.0 (0.0)	1776, 254, 351
	$^7\Sigma^+$	2.281	1.241	12.00	77.3 (84.6)	1659, 149, 262
$TaCN^-$	$^4\Delta$	2.101	1.189	3.750	–	1946, 275, 374
TaCN	$^5\Delta$	2.073	1.182	6.000	–	2007, 246, 410
BO^-	$^1\Sigma^+$	–	1.247	0.000	–	1675
BO	$^2\Sigma^+$	–	1.216	0.750	–	1839
CN^-	$^1\Sigma^+$	–	1.183	0.000	–	2046
CN	$^2\Sigma^+$	–	1.175	0.750	–	2080

[a]R is the bond length, $\langle S^2\rangle$ is the final spin from BP86 calculations, and ΔE is the energy relative to the lowest state. The isoelectronic tantalum cyanide and free $BO^{-/0}$ and $CN^{-/0}$ are also calculated to compare with the boronyl cluster. [b]These values are calculated using BP86 with the Stuttgart basis set for Ta and aug-cc-pVTZ basis set for B and O. The values in parentheses are calculated using CCSD(T) with the same basis sets using the optimized geometries from the BP86 calculations. [c]This state has significant spin contamination, so there may be larger errors for the calculated values.

computed using different methods are summarized in Tables S2 and S3, respectively.

The ground state of $TaBO^-$ ($^4\Delta$) has an electron configuration of $1\sigma^2 2\sigma^2 1\pi^4 3\sigma^2 4\sigma^2 2\pi^2 1\delta^1$; and the valence molecular orbital (MO) pictures are shown in Figure 2. A MO correlation diagram is shown in Figure 3. The electronic structure of $TaBO^-$ is similar to that of the isoelectronic TaCO.[42−45] The relative energies of several electronic states of neutral TaBO are given in Table 2 at the BP86 and CCSD(T) levels of theory. The ground state of TaBO was found to be the $^5\Delta$ state by removal of an electron from the 4σ orbital of $TaBO^-$.

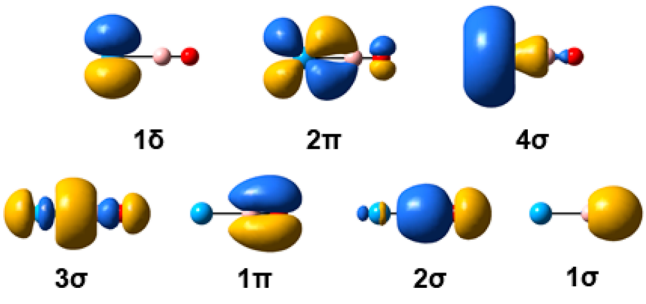

Figure 2. Molecular orbital pictures for $TaBO^-$ plotted with an isovalue of 0.030 e/bohr.[3]

6. DISCUSSION

6.1. Spectral Assignments. Peak X is due to the transition from the anion ground state ($^4\Delta$) to that of the neutral ($^5\Delta$). The calculated ADE of 1.64 eV at the CCSD(T) level is in reasonable agreement with the experimental value of 1.729 eV. The B3LYP, BP86, and PW91PW91 methods also produced theoretical ADEs in good agreement with peak X for the $^5\Delta \leftarrow {}^4\Delta$ transition (Table S4). The separations of peaks A and B from X cannot be explained by vibrational excitations; they are most likely due to transitions to the excited spin−orbit states ($^5\Delta_1$ and $^5\Delta_2$, respectively) of neutral TaBO with peak X corresponding to the $^5\Delta_0$ ground state. The transitions to the $^5\Delta_3$ and $^5\Delta_4$ spin−orbit states at higher energies might be too weak to be observed. The $^5\Delta \leftarrow {}^4\Delta$ transition results from the detachment of an electron from the 4σ orbital, which is mainly of Ta 6s character (Figures 2 and 3). The observed β values shown in Table 1 increase above 1.0 at higher kinetic energies and represent an outgoing *p*-wave, which is consistent with the MO character.

https://dx.doi.org/10.1021/acs.jpca.0c09196
J. Phys. Chem. A 2020, 124, 10001−10007

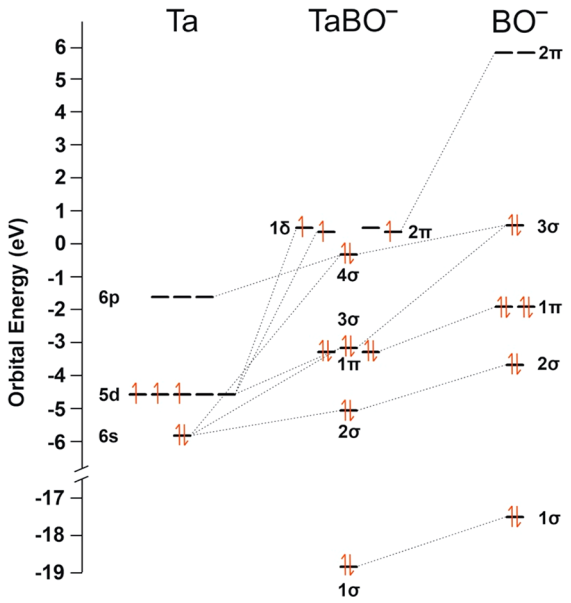

Figure 3. Valence molecular orbital correlation diagram for $TaBO^-$. The orbital energies were computed at the BP86 level of theory with the aug-cc-pVTZ (B and O) and Stuttgart (Ta) basis sets.

The weak peaks observed between peaks X, A, and B should be due to vibrational structures of each spin−orbit state. The higher resolution spectrum in Figure 1a shows that the peaks associated with A and B are split. Even though the peak associated with the X peak at 1.766 eV was not resolved, it was deconvoluted with two Gaussian peaks to yield an identical splitting as the weak peaks associated with A and B (Table S1). The larger vibrational frequency of 320 cm^{-1} agrees well with the calculated value of 351 cm^{-1} for the Ta−B stretching mode (ν_3) for the $^5\Delta$ ground state. The observation of this mode is consistent with the calculations and the MO picture in Figure 2: the electron is detached from the 4σ orbital, which is slightly antibonding between Ta and B, leading to a decreased Ta−B bond length in the neutral (Table 2). The smaller frequency of 240 cm^{-1} agrees well with the calculated bending frequency of 254 cm^{-1} for the ground state. Due to symmetry selection rules, only totally symmetric modes are normally observed in PES experiments. However, vibronic coupling with nearby electronic states can break these selection rules, making excitation of the bending mode possible.[67−69]

The next detachment channel is from the 1δ orbital, resulting in the $^3\Sigma^+$ state, which is assigned to peak C. The calculated ADE for this detachment channel was 1.86 eV at the CCSD(T) level and 2.26 eV at BP86 level, in good agreement with the ADE measured for peak C at 1.947 eV (Table 1). The relatively weak intensity of peak C is consistent with the detachment from the high angular momentum 1δ orbital. Peaks D and E are assigned to the $^3\Delta$ state due to detachment from the 2π orbital. Again, spin−orbit coupling can split the $^3\Delta$ state into $^3\Delta_1$, $^3\Delta_2$, and $^3\Delta_3$ and peaks D and E correspond to the $^3\Delta_1$ and $^3\Delta_2$ states, respectively. Detachment features for the $^3\Delta_3$ state could correspond to the features above 2.1 eV, where numerous peaks were observed in the 532.0 nm spectrum (Figure 1b). The averaged vibrational frequency of peaks D and E is 320 ± 40 cm^{-1}, consistent with the calculated Ta−B stretching mode of the $^3\Delta$ state of 350 cm^{-1}. The calculated ADE without considering spin−orbit coupling seems overestimated in comparison to the experimental data for the $^3\Delta$ state (Table 1).

The X′ and A′ peaks at lower binding energies were broad and likely came from combinations of vibrational and spin−orbit excited states of the anion. The spacing of the main X′ and A′ features (~490 cm^{-1}) is similar to the spacing of X and A (Table 1), suggesting they should have the same final states ($^5\Delta_0$ and $^5\Delta_1$). The ground state of $TaBO^-$ should be $^4\Delta_{1/2}$ with a low-lying $^4\Delta_{3/2}$ spin−orbit exited state, which gives rise to X′ and A′ (Table 1). The spacing between the X and X′ peaks (~670 cm^{-1}) should represent the separation between the $^4\Delta_{1/2}$ and $^4\Delta_{3/2}$ states.

6.2. Comparison of the Structures between $TaBO^{-/0}$ and $TaCN^{-/0}$. While the current results show the ground sate of $TaBO^-$ is the $^4\Delta$ state, the ground state of the isoelectronic $TaCN^-$ is not known. We calculated the $^4\Delta$ state (and $^5\Delta$ for neutral TaCN) in order to make a direct comparison to $TaBO^{-/0}$. One reason that the BO^- unit is not a good ligand for metal atoms is due to the fact that its π^* LUMO is much higher in energy compared to that of CO and CN^-.[1] This means that the metal d_{xz} and d_{yz} orbitals cannot participate effectively in π-backbonding with BO. One indication of π-backbonding in BO (or CN) is the decrease in the BO (or CN) stretching frequency due to the donation of electron density to the π^* orbitals of BO or CN, weakening the ligand bond. Although we did not experimentally observe the B−O stretching frequency, there is a clear decrease in the calculated frequency from 1839 cm^{-1} for free BO to 1776 cm^{-1} in the ground state of TaBO (Table 2). Additionally, there is an increase of 0.016 Å for the calculated BO bond length in TaBO. We also calculated the CN stretching frequency of 2007 cm^{-1} in TaCN compared to 2080 cm^{-1} for CN and a small bond length increase of 0.007 Å. This indicates there should be π-backbonding in both TaBO and TaCN. Comparison of the B−O frequency and bond length in $TaBO^-$ to those of free BO^- seems to indicate that there is no or much weaker back bonding in $TaBO^-$. However, other analyses shown below suggest there is backdonation present in $TaBO^-$, albeit weaker than that in the TaBO neutral.

The estimated bond length for a Ta−B single bond is 2.31 Å while the Ta═B double bond is 2.04 Å using Pyykkö's covalent radii.[70] Our calculated Ta−B bond length in neutral TaBO is 2.110 Å, which is closer to a double bond (Table 2). Likewise, the calculated Ta−B bond in $TaBO^-$ is 2.21 Å, which is still shorter than a single bond. The 3σ and 4σ are bonding and antibonding orbitals so there must be some additional bonding from the backdonation in the 2π orbital causing this bond length to be shorter than a single bond. This observation suggests that there should be backdonation from $5d_{xz}$ or $5d_{yz}$ orbitals of Ta to the π^* orbital of the BO, as represented by the 2π orbital (Figure 2). Similarly, the computed Ta−C bond lengths in $TaCN^{-/0}$ (2.101 and 2.073 Å) are between the estimated double and single Ta−C bond lengths of 1.95 and 2.21 Å, respectively. Previous calculations on $PtBO^{-/0}$ and $PdBO^{-/0}$ showed $BO^{-/0}$ are weak π acceptors relative to $CN^{-/0}$.[37] This is consistent with our results for $TaBO^{-/0}$. The calculated Pt−B and Pd−B bond lengths are also close to the estimated Pt═B and Pd═B double bond lengths.[37]

6.3. Analyses of Natural Atomic Orbitals, Bond Orders, and Dissociation Energies. We performed a natural atomic orbital (NAO) analysis[71] on $TaBO^{-/0}$ and $TaCN^{-/0}$ to provide a more quantitative measure of the π-backdonation. A summary of the higher energy α 2π orbitals

https://dx.doi.org/10.1021/acs.jpca.0c09196
J. Phys. Chem. A 2020, 124, 10001−10007

Table 3. Natural Atomic Orbital Analyses for the 2π Orbitals of $TaBO^-$ and TaBO Compared with the Isoelectronic Tantalum Cyanides[a]

molecule	atom	atomic orbital	contribution (%)	molecule	atom	atomic orbital	contribution (%)
$TaBO^-$	Ta	$5d_{xz}$	87.1	$TaCN^-$	Ta	$5d_{xz}$	84
	B	$2p_x$	6.4		C	$2p_x$	1.9
	O	$2p_x$	6.3		N	$2p_x$	14
TaBO	Ta	$5d_{xz}$	88.8	TaCN	Ta	$5d_{xz}$	84
	B	$2p_x$	3.2		C	$2p_x$	0.2
	O	$2p_x$	7.8		N	$2p_x$	15

[a]The perpendicular orbitals ($5d_{yz}$ and $2p_y$) showed identical contributions.

Table 4. Calculated Bond Orders for $TaBO^{-/0}$ and the Isoelectronic Tantalum Cyanides Using the Fuzzy Bond Order (FBO)[a]

molecule	bond	FBO[b]	dissociation reaction	BDE[b] (kcal/mol)	BDE[c] (kcal/mol)
$TaBO^-$	Ta−B	1.29	$TaBO^-$ ($^4\Delta$) → Ta (^{4}F) + BO^- ($^1\Sigma^+$)	59.9	63.6
	B−O	2.13			
TaBO	Ta−B	1.20	TaBO ($^5\Delta$) → Ta (^{4}F) + BO ($^2\Sigma^+$)	81.2	82.7
	B−O	2.20			
$TaCN^-$	Ta−C	1.45	$TaCN^-$ ($^4\Delta$) → Ta (^{4}F) + CN^- ($^1\Sigma^+$)	59.8	63.6
	C−N	2.59			
TaCN	Ta−C	1.42	TaCN ($^5\Delta$) → Ta (^{4}F) + CN ($^2\Sigma^+$)	107.5	111.9
	C−N	2.59			
BO^-	B−O	2.41	–	–	–
BO	B−O	2.49	–	–	–
CN^-	C−N	3.05	–	–	–
CN	C−N	3.18	–	–	–

[a]Bond dissociation energies (BDEs) are also presented for the lowest energy Ta−B and Ta−C dissociation reactions. [b]Calculated using the BP86 functional with the Stuttgart (Ta) and aug-cc-pVTZ (B and O) basis sets. [c]Calculated from single point calculations using the BP86 optimized geometries with CCSD(T) and the Stuttgart (Ta) and aug-cc-pVTZ (B and O) basis sets.

for $TaBO^{-/0}$ and $TaCN^{-/0}$ are given in Table 3. The NAO analyses of all valence orbitals are presented in the Supporting Information (Table S5). The composition of both 2π orbitals in neutral and anionic TaBO clearly show that the antibonding π^* orbital of BO contributes just over 10% to the molecular orbitals. The NAO results for the isoelectronic $TaCN^-$ species show that the CN^- antibonding π^* orbitals contribute 16% to the 2π MO.

Additionally, we computed the Fuzzy bond order[72] for each molecule along with free $CN^{-/0}$ and $BO^{-/0}$. In all cases the Ta−B and Ta−C bonds are slightly above 1 and the B−O and C−N bond orders decrease compared to free $CN^{-/0}$ and $BO^{-/0}$, showing a strengthening of the metal−boron or metal−carbon bond and weakening of the ligand bond. The computed bond dissociation energies (BDEs) in Table 4 are nearly identical for $TaBO^-$ and $TaCN^-$, consistent with their similar bonding. There is a larger difference in the BDEs of the two neutral species, which is likely due to the degree of antibonding in the 4σ orbital. The larger BDE in TaCN indicates that the 4σ orbital is more antibonding compared to TaBO. These results show that the π-backbonding is similar in both the boronyl and cyanide ligands, suggesting early 5d transition metals are quite suitable to form highly stable boronyl compounds.

7. CONCLUSIONS

We present the first observation of a boronyl ligand bonded to an early transition metal. Photoelectron spectra at two wavelengths were measured using photoelectron imaging. The ground state of $TaBO^-$ is determined to be $^4\Delta_{1/2}$ while the neutral ground state is $^5\Delta_0$. Spin−orbit splitting is observed for the ground and second excited state of neutral TaBO and vibrational information is observed for these states. The calculated bond lengths, NAO analyses, and bond orders show that there is π-backbonding to stabilize the boronyl ligand comparable to the isoelectronic cyanide ligands. The observation of π-backbonding suggests that early 5d transition metals are promising to form stable boronyl compounds.

■ ASSOCIATED CONTENT

Supporting Information

The Supporting Information is available free of charge at https://pubs.acs.org/doi/10.1021/acs.jpca.0c09196.

Summary of all experimentally observed peaks, theoretical results at all levels of theory used, and the full NAO analyses for $TaBO^{-/0}$ and $TaCN^{-/0}$ (PDF)

■ AUTHOR INFORMATION

Corresponding Author

Lai-Sheng Wang − *Department of Chemistry, Brown University, Providence, Rhode Island 02912, United States;* orcid.org/0000-0003-1816-5738; Email: Lai-Sheng_Wang@brown.edu

Author

Joseph Czekner − *Department of Chemistry, Brown University, Providence, Rhode Island 02912, United States*

Complete contact information is available at: https://pubs.acs.org/10.1021/acs.jpca.0c09196

Notes

The authors declare no competing financial interest.

■ ACKNOWLEDGMENTS

This work was supported by the National Science Foundation (CHE-1763380). We also acknowledge Brown University's Center for Computation and Visualization for the use of their computer clusters.

■ REFERENCES

(1) Ehlers, A. W.; Baerends, E. J.; Bickelhaupt, F. M.; Radius, U. Alternatives to the CO Ligand: Coordination of the Isolobal Analogues BF, BNH_2, $BN(CH_3)_2$, and BO^- in Mono- and Binuclear First-Row Transition Metal Complexes. *Chem. - Eur. J.* **1998**, *4*, 210−221.

(2) Bock, H.; Cederbaum, L.; von Niessen, W.; Paetzold, P.; Rosmus, P.; Solouki, B. Methylboron Oxide, H_3C-BO. *Angew. Chem., Int. Ed. Engl.* **1989**, *28*, 88−90.

(3) Zhai, H. J.; Chen, Q.; Bai, H.; Li, S. D.; Wang, L. S. Boronyl Chemistry: The BO Group as a New Ligand in Gas-Phase Clusters and Synthetic Compounds. *Acc. Chem. Res.* **2014**, *47*, 2435−2445.

(4) Zhai, H. J.; Li, S. D.; Wang, L. S. Boronyls as Key Structural Units in Boron Oxide Clusters: $B(BO)_2^-$ and $B(BO)_3^-$. *J. Am. Chem. Soc.* **2007**, *129*, 9254−9255.

(5) Li, S. D.; Zhai, H. J.; Wang, L. S. $B_2(BO)_2^-$ - Diboronyl Biborene: A Linear Molecule with a Triple Boron-Boron Bond. *J. Am. Chem. Soc.* **2008**, *130*, 2573−2579.

(6) Chen, Q.; Zhai, H. J.; Li, S. D.; Wang, L. S. Probing the Structures and Chemical Bonding of Boron-Boronyl Clusters Using Photoelectron Spectroscopy and Computational Chemistry: $B_4(BO)_n^-$ (n = 1−3). *J. Chem. Phys.* **2012**, *137*, No. 044307.

(7) Chen, Q.; Bai, H.; Zhai, H. J.; Li, S. D.; Wang, L. S. Photoelectron Spectroscopy of Boron-Gold Alloy Clusters and Boron Boronyl Clusters: B_3Au_n and $B_3(BO)_n$ (n = 1, 2). *J. Chem. Phys.* **2013**, *139*, No. 044308.

(8) Zhai, H. J.; Miao, C. Q.; Li, S. D.; Wang, L. S. On the Analogy of B-BO and B-Au Chemical Bonding in $B_{11}O^-$ and $B_{10}Au^-$ Clusters. *J. Phys. Chem. A* **2010**, *114*, 12155−12161.

(9) Bai, H.; Zhai, H. J.; Li, S. D.; Wang, L. S. Photoelectron Spectroscopy of Aromatic Compound Clusters of the B_{12} All-Boron Benzene: $B_{12}Au^-$ and $B_{12}(BO)^-$. *Phys. Chem. Chem. Phys.* **2013**, *15*, 9646−9653.

(10) Zhai, H.-J.; Chen, Q.; Bai, H.; Lu, H.-G.; Li, W.-L.; Li, S.-D.; Wang, L.-S. Pi and Sigma Double Conjugations in Boronyl Polyboroene Nanoribbons: $B_n(BO)_2^-$ and $B_n(BO)_2$ (n = 5−12). *J. Chem. Phys.* **2013**, *139*, 174301.

(11) Nguyen, M. T.; Matus, M. H.; Ngan, V. T.; Grant, D. J.; Dixon, D. A. Thermochemistry and Electronic Structure of Small Boron and Boron Oxide Clusters and Their Anions. *J. Phys. Chem. A* **2009**, *113*, 4895−4909.

(12) Tai, T. B.; Nguyen, M. T.; Dixon, D. A. Thermochemical Properties and Electronic Structure of Boron Oxides B_nO_m (n = 5−10, m = 1, 2) and Their Anions. *J. Phys. Chem. A* **2010**, *114*, 2893−2912.

(13) Zhai, H. J.; Guo, J. C.; Li, S. D.; Wang, L. S. Bridging η^2-BO in $B_2(BO)_3^-$ and $B_3(BO)_3^-$ Clusters: Boronyl Analogs of Boranes. *ChemPhysChem* **2011**, *12*, 2549−2553.

(14) Zubarev, D. Y.; Boldyrev, A. I.; Li, J.; Zhai, H. J.; Wang, L. S. On the Chemical Bonding of Gold in Auro-Boron Oxide Clusters Au_nBO^- (n = 1−3). *J. Phys. Chem. A* **2007**, *111*, 1648−1658.

(15) Miao, C. Q.; Lu, H. G.; Li, S. D. Covalent Bonding in $Au(BO)_2^-$ and $Au(BS)_2^-$. *J. Cluster Sci.* **2013**, *24*, 233−241.

(16) Jian, T.; Lopez, G. V.; Wang, L. S. Photoelectron Spectroscopy of $BiAu^-$ and $BiBO^-$: Further Evidence of the Analogy between Au and Boronyl. *J. Phys. Chem. B* **2016**, *120*, 1635−1640.

(17) Jian, T.; Cheung, L. F.; Chen, T. T.; Wang, L. S. Bismuth-Boron Multiple Bonding in BiB_2O^- and Bi_2B^-. *Angew. Chem., Int. Ed.* **2017**, *56*, 9551−9555.

(18) Mason, J. L.; Harb, H.; Topolski, J. E.; Hratchian, H. P.; Jarrold, C. C. A Tale of Two Stabilities: How One Boron Atom Affects a Switch in Bonding Motifs in $CeO_2B_x^-$ (x = 2, 3) Complexes. *J. Phys. Chem. A* **2018**, *122*, 9879−9885.

(19) Cheung, L. F.; Chen, T. T.; Kocheril, G. S.; Chen, W. J.; Czekner, J.; Wang, L. S. Observation of Four-Fold Boron-Metal Bonds in $RhB(BO^-)$ and RhB. *J. Phys. Chem. Lett.* **2020**, *11*, 659−663.

(20) Chen, T. T.; Cheung, L. F.; Chen, W. J.; Cavanagh, J.; Wang, L. S. Observation of Transition-Metal-Boron Triple Bonds in IrB_2O^- and ReB_2O^-. *Angew. Chem., Int. Ed.* **2020**, *59*, 15260−15265.

(21) Parker, D. S. N.; Zhang, F.; Maksyutenko, P.; Kaiser, R. I.; Chang, A. H. H. A Crossed Beam and *ab initio* Investigation of the Reaction of Boron Monoxide (^{11}BO; $X\ ^2\Sigma^+$) with Acetylene (C_2H_2; $X\ ^1\Sigma_g^+$). *Phys. Chem. Chem. Phys.* **2011**, *13*, 8560−8570.

(22) Maity, S.; Parker, D. S. N.; Dangi, B. B.; Kaiser, R. I.; Fau, S.; Perera, A.; Bartlett, R. J. A Crossed Molecular Beam and Ab-Initio Investigation of Boron Monoxide (BO; $X\ ^2\Sigma^+$) with Methylacetylene (CH_3CCH; $X\ ^1A_1$): Competing Atomic Hydrogen and Methyl Loss Pathways. *J. Phys. Chem. A* **2013**, *117*, 11794−11807.

(23) Kaiser, R. I.; Balucani, N. Exploring the Gas Phase Synthesis of the Elusive Class of Boronyls and the Mechanism of Boronyl Radical Reactions under Single Collision Conditions. *Acc. Chem. Res.* **2017**, *50*, 1154−1162.

(24) Braunschweig, H.; Radacki, K.; Schneider, A. Oxoboryl Complexes: Boron-Oxygen Triple Bonds Stabilized in the Coordination Sphere of Platinum. *Science* **2010**, *328*, 345−347.

(25) Kaneko, T.; Takao, T.; Suzuki, H. A Triruthenium Complex Capped by a Triply Bridging Oxoboryl Ligand. *Angew. Chem., Int. Ed.* **2013**, *52*, 11884−11887.

(26) Tian, W. J.; Zhao, L. J.; Chen, Q.; Ou, T.; Xu, H. G.; Zheng, W. J.; Zhai, H. J.; Li, S. D. Photoelectron Spectroscopy of $B_4O_4^-$: Dual 3c-4e π Hyperbonds and Rhombic 4c-4e o-bond in Boron Oxide Clusters. *J. Chem. Phys.* **2015**, *142*, 134305.

(27) Zhao, L. J.; Tian, W. J.; Ou, T.; Xu, H. G.; Feng, G.; Xu, X. L.; Zhai, H. J.; Li, S. D.; Zheng, W. J. Structures and Chemical Bonding of $B_3O_3^{-/0}$ and $B_3O_3H^{-/0}$: A Combined Photoelectron Spectroscopy and First-Principles Theory Study. *J. Chem. Phys.* **2016**, *144*, 124301.

(28) Gong, X.; Li, Q. S.; Xie, Y.; King, R. B.; Schaefer, H. F., III Boronyl Ligand as a Member of the Isoelectronic Series $BO^- \rightarrow CO \rightarrow NO^+$: Viable Cobalt Carbonyl Boronyl Derivatives? *Inorg. Chem.* **2010**, *49*, 10820−10832.

(29) Chang, Y.; Li, Q. S.; Xie, Y.; King, R. B. Prospects for Three-Electron Donor Boronyl (BO) Ligands and Dioxodiborene (B_2O_2) Ligands as Bridging Groups in Binuclear Iron Carbonyl Derivatives. *Inorg. Chem.* **2012**, *51*, 8904−8915.

(30) Zeng, G.; Sakaki, S. Theoretical Study on the Transition-Metal Oxoboryl Complex: M-BO Bonding Nature, Mechanism of the Formation Reaction, and Prediction of a New Oxoboryl Complex. *Inorg. Chem.* **2012**, *51*, 4597−4605.

(31) Zhang, Z.; Pu, L.; Li, Q. S.; King, R. B. Pathways to the Polymerization of Boron Monoxide Dimer to Give Low-Density Porous Materials Containing Six-Membered Boroxine Rings. *Inorg. Chem.* **2015**, *54*, 2910−2915.

(32) Wang, H.; Chen, Q.; Wang, Y. J.; Bai, H.; Gao, T. T.; Li, H. R.; Zhai, H. J.; Li, S. D. Boronyl as a Terminal Ligand in Boron Oxide Clusters: Hexagonal Ring C_{2v} B_6O_4 and Ethylene-like D_{2h} $B_6O_4^{-/2-}$. *Phys. Chem. Chem. Phys.* **2015**, *17*, 19929−19935.

(33) Zhang, Z.; Pu, L.; Li, Q. S.; King, R. B. The Siliconyl, Boronyl, and Iminoboryl Ligands as Analogues of the Well-known Carbonyl Ligand: Predicting Reactivity towards Dipolar Cyclooligomerization in Iron/Cobalt Carbonyl Complexes. *RSC Adv.* **2015**, *5*, 35558−35563.

(34) Zhang, Z.; Pu, L.; Li, Q. S.; King, R. B. Controlling the Reactivity of the Boronyl Group in Platinum Complexes toward Cyclodimerization: A Theoretical Study. *Inorg. Chem.* **2015**, *54*, 10281−10286.

(35) Liu, Y.; Liu, C.; Pu, L.; Zhang, Z.; King, R. B. Boron Monoxide Dimer as a Building Block for Boroxine Based Buckyballs and Related Cages: A Theoretical Study. *Chem. Commun.* **2017**, *53*, 3239−3241.

(36) Vega-Vega, Á.; Barrientos, C.; Largo, A. Metallic Monoboronyl Compounds: Prediction of Their Structure and Comparison with the Cyanide Analogues. *J. Comput. Chem.* **2017**, *38*, 807−815.

https://dx.doi.org/10.1021/acs.jpca.0c09196
J. Phys. Chem. A 2020, 124, 10001−10007

(37) Moon, J.; Kim, J. Theoretical Investigation of the Molecular Properties of PtBO and PdBO. *Comput. Theor. Chem.* **2017**, *1108*, 23−28.
(38) Moon, J.; Baek, H.; Kim, J. Unusually High Stability of $B_{12}(BO)_{12}^{2-}$ Achieved by Boronyl Ligand Manipulation: Theoretical Investigation. *Chem. Phys. Lett.* **2018**, *698*, 72−76.
(39) León, I.; Yang, Z.; Liu, H. T.; Wang, L. S. The Design and Construction of A High-Resolution Velocity-Map Imaging Apparatus for Photoelectron Spectroscopy Studies of Size-Selected Clusters. *Rev. Sci. Instrum.* **2014**, *85*, No. 083106.
(40) Dick, B. Inverting Ion Images with Abel Inversion: Maximum Entropy Reconstruction of Velocity Maps. *Phys. Chem. Chem. Phys.* **2014**, *16*, 570−580.
(41) Frisch, M. J.; Trucks, G. W.; Schlegal, H. B.; Scuseria, G. E.; Robb, M. A.; Cheeseman, J. R.; Scalmani, G.; Barone, V.; Petersson, G. A.; Nakatsuji, H.; et al., *Gaussian 09*, Rev. C.01; Gaussian, Inc.: Wallingford, CT, 2016.
(42) Zhou, M.; Andrews, L. Infrared Spectra of CNbO, CMO^-, OMCCO, $(C_2)MO_2$, and $M(CO)_x$ (x = 1−6) (M = Nb, Ta) in Solid Neon. *J. Phys. Chem. A* **1999**, *103*, 7785−7794.
(43) Lu, Z. H.; Jiang, L.; Xu, Q. Infrared Spectra and Density Functional Theory Calculations of the Tantalum and Niobium Carbonyl Dinitrogen Complexes. *J. Chem. Phys.* **2009**, *131*, No. 034512.
(44) Majumdar, D.; Balasubramanian, K. A Theoretical Study of the Curves for Ta + CO Interaction. *Chem. Phys. Lett.* **1996**, *262*, 263−268.
(45) Wu, Z. J.; Li, H. L.; Zhang, H. J.; Meng, J. Electronic Structures of MCO (M = Nb, Ta, Rh, Ir, Pd, Pt) Molecules by Density Functional Theory. *J. Phys. Chem. A* **2004**, *108*, 10906−10910.
(46) Becke, A. D. Density-Functional Thermochemistry. IV. A New Dynamical Correlation Functional and Implications for Exact-Exchange Mixing. *J. Chem. Phys.* **1996**, *104*, 1040−1046.
(47) Adamo, C.; Barone, V. Toward Reliable Adiabatic Connection Models Free From Adjustable Parameters. *Chem. Phys. Lett.* **1997**, *274*, 242−250.
(48) Perdew, J. P.; Burke, K.; Ernzerhof, M. Generalized Gradient Approximation Made Simple. *Phys. Rev. Lett.* **1996**, *77*, 3865−3868.
(49) Perdew, J. P.; Burke, K.; Ernzerhof, M. Generalized Gradient Approximation Made Simple [Errata]. *Phys. Rev. Lett.* **1997**, *78*, 1396.
(50) Adamo, C.; Barone, V. Toward Reliable Density Functional Methods Without Adjustable Parameters: The PBE0Model. *J. Chem. Phys.* **1999**, *110*, 6158−6170.
(51) Perdew, J. P. *Electronic Structure of Solids*; Akademie Verlag: Berlin, Germany, 1991.
(52) Perdew, J. P. Density-Functional Approximations for the Correlation Energy of the Inhomogeneous Electron Gas. *Phys. Rev. B: Condens. Matter Mater. Phys.* **1986**, *33*, 8822−8824.
(53) Becke, A. D. Density-Functional Exchange-Energy Approximation with Correct Asymptotic Behavior. *Phys. Rev. A: At., Mol., Opt. Phys.* **1988**, *38*, 3098−3100.
(54) Hehre, W. J.; Ditchfield, R.; Pople, J. A. Self-Consistent Molecular Orbital Methods. XII. Further Extensions of Gaussian-Type Basis Sets for Use in Molecular Orbital Studies of Orgranic Molecules. *J. Chem. Phys.* **1972**, *56*, 2257−2261.
(55) Clark, T.; Chandrasekhar, J.; Spitznagel, G. W.; Schleyer, P. v. R. Efficient Diffuse Function-Augmented Basis Sets for Anion Calculations. III. The 3-21+g Basis Set for First-Row Elements, Li-F. *J. Comput. Chem.* **1983**, *4*, 294−301.
(56) Kendall, R. A.; Dunning, T. H., Jr.; Harrison, R. J. Electron Affinities of the First-Row Atoms Revisited: Systematic Basis Sets and Wave Functions. *J. Chem. Phys.* **1992**, *96*, 6796−6808.
(57) Hay, P. J.; Wadt, W. R. *Ab initio* Effective Core Potentials for Molecular Calculations. *J. Chem. Phys.* **1985**, *82*, 270−283.
(58) Hay, P. J.; Wadt, W. R. *Ab initio* Effective Core Potentials for Molecular Calculations. Potentials for K to Au including the Outermost Core Orbitals. *J. Chem. Phys.* **1985**, *82*, 299−310.
(59) Andrae, D.; Haeußermann, U.; Dolg, M.; Stoll, H.; Preuß, H. Energy-Adjusted *ab initio* Pseudopotentials for the Second and Third Row Transition Elements. *Theor. Chem. Acc.* **1990**, *77*, 123−141.
(60) Martin, J. M. L.; Sundermann, A. Correlation Consistent Valence Basis Sets for use With the Stuttgart-Dresden-Bonn Relativistic Effective Core Potentials: The Atoms Ga-Kr and In-Xe. *J. Chem. Phys.* **2001**, *114*, 3408−3420.
(61) Xie, L.; Li, W. L.; Romanescu, C.; Huang, X.; Wang, L. S. A Photoelectron Spectroscopy and Density Functional Study of Di-Tantalum Boride Clusters: $Ta_2B_x^-$ (*x* = 2−5). *J. Chem. Phys.* **2013**, *138*, No. 034308.
(62) Li, W. L.; Ivanov, A. S.; Federic, J.; Romanescu, C.; Cernusak, I.; Boldyrev, A. I.; Wang, L. S. On the Way to the Highest Coordination Number in the Planar Metal-Centered Aromatic $Ta©B_{10}^-$ Cluster: Evolution of the Structures of TaB_n^- (*n* = 3−8). *J. Chem. Phys.* **2013**, *139*, 104312.
(63) Li, W. L.; Xie, L.; Jian, T.; Romanescu, C.; Huang, X.; Wang, L. S. Hexagonal Bipyramidal $Ta_2B_6^{-/0}$ Clusters: B_6 Rings as Structural Motifs. *Angew. Chem.* **2014**, *126*, 1312−1316.
(64) Purvis, G. D.; Bartlett, R. J. A Full Couple-Cluster Singles and Doubles Model: The Inclusion of Disconnected Triples. *J. Chem. Phys.* **1982**, *76*, 1910−1918.
(65) Scuseria, G. E.; Janssen, C. L.; Schaefer, H. F., III An Efficient Reformulation of the Close-Shell Coupled Cluster Single and Double Excitation (CCSD) Equations. *J. Chem. Phys.* **1988**, *89*, 7382−7387.
(66) Pople, J. A.; Head-Gordon, M.; Raghavachari, K. Quadratic Configuration Interaction. A General Technique for Determining Electron Correlation Energies. *J. Chem. Phys.* **1987**, *87*, 5968−5975.
(67) Northrup, F. J.; Sears, T. J. Renner-Teller, Spin-Orbit, and Fermi-Resonance Interactions in *X* $^2\Pi$ NCS Investigated by LIF Spectroscopy. *Mol. Phys.* **1990**, *71*, 45−64.
(68) Presunka, P. I.; Coxon, J. A. Laser Spectroscopy of the $\tilde{A}\,^2\Pi$- $\tilde{X}\,^2\Sigma^+$ Transition of SrOH: Deperturbation Analysis of *K*-Resonance in the ν_2=1 Level of the $\tilde{A}\,^2\Pi$ State. *J. Chem. Phys.* **1994**, *101*, 201−222.
(69) He, S. G.; Li, H.; Smith, T. C.; Clouthier, D. J.; Merer, A. J. The Renner-Teller Effect and Sears Resonances in the Ground State of the GeCH and GeCD Free Radicals. *J. Chem. Phys.* **2003**, *119*, 10115−10124.
(70) Pyykkö, P. Additive Covalent Radii for Single-, Double-, and Triple-Bonded Molecules and Tetrahedrally Bonded Crystals: A Summary. *J. Phys. Chem. A* **2015**, *119*, 2326−2337.
(71) Reed, A. E.; Weinstock, R. B.; Weinhold, F. Natural Population Analysis. *J. Chem. Phys.* **1985**, *83*, 735−746.
(72) Mayer, I.; Salvador, P. Overlap Populations, Bond Orders and Valences for 'Fuzzy' Atoms. *Chem. Phys. Lett.* **2004**, *383*, 368−375.

https://dx.doi.org/10.1021/acs.jpca.0c09196
J. Phys. Chem. A 2020, 124, 10001−10007